JACS ARTICLES

Published on Web 10/01/2009

Activation of the S−H Group in Fe(μ_2-SH)Fe Clusters: S−H Bond Strengths and Free Radical Reactivity of the Fe(μ_2-SH)Fe Cluster

James A. Franz,*,† Suh-Jane Lee,† Thomas A. Bowden,† Mikhail S. Alnajjar,† Aaron M. Appel,† Jerome C. Birnbaum,† Thomas E. Bitterwolf,‡ and Michel Dupuis†

Pacific Northwest National Laboratory, P.O. Box 999, Richland, Washington 99352, and Department of Chemistry, University of Idaho, Moscow, Idaho 83844-2343

Received June 10, 2009; E-mail: james.franz@pnl.gov

Abstract: Absolute rate constants were determined for the abstraction of hydrogen atoms from $(OC)_3Fe(\mu\text{-}SH)_2Fe(CO)_3$ (**$Fe_2S_2H_2$**) and $(OC)_3Fe(\mu\text{-}SCH_3)(\mu\text{-}SH)Fe(CO)_3$ (**Fe_2S_2MeH**) by benzyl radicals in benzene. From the temperature-dependent rate data for **$Fe_2S_2H_2$**, $\Delta H^{\ddagger}$ and $\Delta S^{\ddagger}$ were determined to be 2.03 ± 0.56 kcal/mol and −19.3 ± 1.7 cal/(mol K), respectively, giving $k_{abs} = (1.2 \pm 0.49) \times 10^7$ M^{-1} s^{-1} at 25 °C. For **Fe_2S_2MeH**, $\Delta H^{\ddagger}$ and $\Delta S^{\ddagger}$ were determined to be 1.97 ± 0.46 kcal/mol and −18.1 ± 1.5 cal/(mol K), respectively, giving $k_{abs} = (2.3 \pm 0.23) \times 10^7$ M^{-1} s^{-1} at 25 °C. Temperature-dependent rate data are also reported for hydrogen atom abstraction by benzyl radical from thiophenol ($\Delta H^{\ddagger} = 3.62 \pm 0.43$ kcal/mol, $\Delta S^{\ddagger} = -21.7 \pm 1.3$ cal/(mol K)) and H_2S ($\Delta H^{\ddagger} = 5.13 \pm 0.99$ kcal/mol, $\Delta S^{\ddagger} = -24.8 \pm 3.2$ cal/(mol K)), giving k_{abs} at 25 °C of $(2.5 \pm 0.33) \times 10^5$ and $(4.2 \pm 0.51) \times 10^3$ M^{-1} s^{-1}, respectively, both having hydrogen atom abstraction rate constants orders of magnitude slower than those of **$Fe_2S_2H_2$** and **Fe_2S_2MeH**. Thus, **Fe_2S_2MeH** is 100-fold faster than thiophenol, known as a fast donor. All rate constants are reported per abstractable hydrogen atom (k_{abs}/M^{-1} s^{-1}/H). DFT calculations predict S−H bond strengths of 73.1 and 73.2 kcal/mol for **$Fe_2S_2H_2$** and **Fe_2S_2MeH**, respectively. Free energy and NMR chemical shift calculations confirm the NMR assignments and populations of **$Fe_2S_2H_2$** and **Fe_2S_2MeH** isomers. Derived radicals **$Fe_2S_2H^{\bullet}$** and **$Fe_2S_2Me^{\bullet}$** exhibit singly occupied HOMOs with unpaired spin density distributed between the two Fe atoms, a bridging sulfur, and d_σ-bonding between Fe centers. The S−H solution bond dissociation free energy (SBDFE) of **Fe_2S_2MeH** was found to be 69.4 ± 1.7 kcal/mol by determination of its pK_a (16.0 ± 0.4) and the potential for the oxidation of the anion, **$Fe_2S_2Me^{-}$**, of −0.26 ± 0.05 V vs ferrocene in acetonitrile (corrected for dimerization of **$Fe_2S_2Me^{\bullet}$**). This SBDFE for **Fe_2S_2MeH** corresponds to a gas-phase bond dissociation enthalpy (BDE) of 74.2 kcal/mol, in satisfactory agreement with the DFT value of 73.2 kcal/mol. Replacement of the Fe−Fe bond in **Fe_2S_2MeH** with bridging μ-S (**Fe_2S_3MeH**) or μ-CO (**$Fe_2S_2(CO)MeH$**) groups leads to (DFT) BDEs of 72.8 and 66.2 kcal/mol, the latter indicating dramatic effects of the choice of bridge structure on S−H bond strengths. These results provide a model for the reactivity of hydrosulfido sites of low-valent heterogeneous FeS catalysts.

Introduction

Hydrosulfido complexes of transition metals are of great importance in catalytic processes such as hydrogenation, hydrocracking, hydrodeoxygenation, and hydrodesulfurization. The Fe_2S_2 core plays a key role in enzymatic activation of molecular hydrogen in hydrogenase enzymes and is important in nitrogenase enzymes.[1,2] The abundance of FeS clusters likely led to the evolution of critical biochemical functionality on primordial earth.[3] The importance of the reactivity *at bridging sulfides and disulfides* is increasingly recognized for metal sulfides used for hydrogen activation, hydrodesulfurization, hydrogenation of unsaturated C−C bonds,[4] and selective hydrocracking of alkylaromatic structure.[5] In spite of the importance of reactivity at sulfur, very few experimental S−H bond strengths are known for metal hydrosulfides. The only reported experimental S−H bond strengths for metal hydrosulfides are for dimolybdenum tetrasulfide complexes,[6−8] all but one[6] of which are included in our recently developed extensive family of bond strengths for Mo(μ-SH)Mo clusters,[9] in which the S−H bond dissociation enthalpies (BDEs) span the remarkable range of 48−72 kcal/

† Pacific Northwest National Laboratory.
‡ University of Idaho.

(1) Peruzzini, M.; de los Rios, I.; Romerosa, A. Coordination Chemistry of Transition Metals with Hydrogen Chalcogenido Ligands. In *Progress in Inorganic Chemistry*; Karlin, K. D., Ed.; Wiley: New York. 2001; Vol. 49, pp 169−443.
(2) Henderson, R. A. *Chem. Rev.* **2005**, *105*, 2365–2438.
(3) (a) Cody, G. D.; Boctor, N. Z.; Filley, T. R.; Hazen, R. M.; Scott, J. H.; Sharma, A.; Yoder, H. S., Jr. *Science* **2000**, *289*, 1337–1340. (b) Wächtershäuser, G. *Chem. Biodiversity* **2007**, *4*, 584–602. (c) Wächtershäuser, G. *Prog. Biophys. Mol. Biol.* **1992**, *58*, 85.
(4) Kuwata, S.; Hidai, M. *Coord. Chem. Rev.* **2001**, *213*, 211–305.
(5) (a) Li, X.; Hu, S.; Jin, L.; Hu, H. *Energy Fuels* **2008**, *22*, 1126–1129. (b) Wei, X. Y.; Ogata, E.; Zong, Z. M.; Niki, E. *Energy Fuels* **1992**, *6*, 868–869. (c) Wei, X. Y.; Ogata, E.; Zong, Z. M.; Niki, E. *Fuel* **1993**, *72*, 1547–1552.
(6) Appel, A. M.; DuBois, D. L.; Rakowski DuBois, M. *J. Am. Chem. Soc.* **2005**, *127*, 12717–12726.
(7) Appel, A. M.; Lee, S.-J.; Franz, J. A.; DuBois, D. J.; DuBois, M. R.; Twamley, B. *Organometallics* **2009**, *28*, 749–754.
(8) Appel, A. M.; Lee, S. J.; Franz, J. A.; DuBois, D. L.; Rakowski DuBois, M.; Birnbaum, J. C.; Twamley, B. *J. Am. Chem. Soc.* **2008**, *130*, 8940–8951.

 10.1021/ja904602p CCC: $40.75

Scheme 1. Stepwise Homolytic Hydrogen Transfer from a Cluster[a] to an Olefin or Polynuclear Aromatic Initiated by Retro-Disproportionation (k_{RRD})[13]

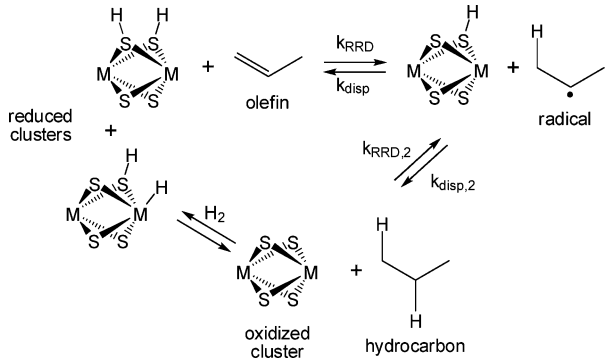

[a] Clusters may be M = Mo, Fe (e.g., pyrrhotite, $Fe_{(1-x)}S$), or mixed metal clusters.

Scheme 2. (Top) Stepwise Homolytic Hydrogen Transfer between Hydrocarbons[13] and (Bottom) Re-initiation of Chain-Transfer Catalysis[18]

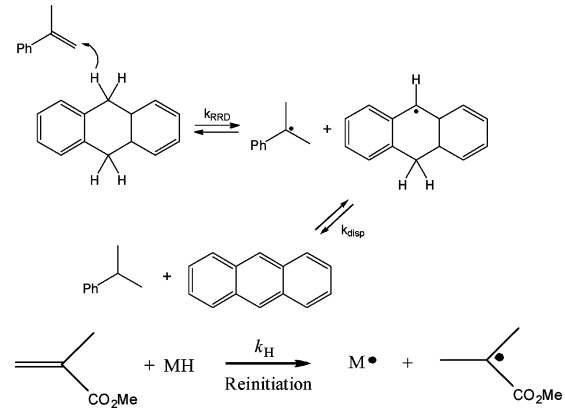

mol. For analogous iron−sulfide complexes, no comparable bond strengths or kinetic measures of S−H reactivity exist. FeS-based heterogeneous catalysts are growing in technological importance in hydrogenation and hydrocracking, specifically for large-scale use in direct coal liquefaction. Iron−sulfide based pyrite- and pyrrhotite-like minerals are solid catalysts for the selective hydrogenation and hydrocracking of alkyl-substituted aromatic organic compounds. These catalysts facilitate selective hydrogenation of aromatic hydrocarbons and hydrocracking of alkyl side chains of aromatic structures.

While the complex structure of pyrrhotite group minerals has been explored,[10] the structural forms of catalytic intermediates in hydrogenation and hydrocracking remain mostly speculative. Early attempts at molecular orbital calculations for iron catalysts revealed the dissociation of H_2 to occur on a stepped $(10\bar{1}0)$ FeS surface, producing a "pseudo-H_2S" species.[11] The further evolution of the H_2-activated structure and participation in hydrogen transfer to acceptor molecules was not addressed. The key hydrogen-transfer step from hydrogen-carrying $Fe_{(1-x)}S$ catalysts may occur by direct hydrogen atom transfer (reverse-radical disproportionation (RRD), or retro-disproportionation) from the reduced FeS catalyst, as depicted in Schemes 1 and 2. The retro-disproportionation mechanism is well characterized for homogeneous hydrogen transfer between organic hydrogen donors and acceptors and is recognized as a primary initiation and hydrogen-transfer pathway in hydropyrolysis of aromatic alkyl structures.[12,13] By virtue of the nearly barrierless nature of the reverse disproportionation steps (k_{disp}) in Schemes 1 and 2, knowledge of C−H, S−H, and M−H bond strengths allows estimation of $\Delta H°$ ($\approx \Delta H^{\ddagger}$) and prediction of the upper limit of the forward rates of hydrogen transfer to acceptor molecules. The retro-disproportionation mechanism is also well established as a means of hydrogen atom transfer from organometallic hydrides with weak M−H bonds to reactive olefinic acceptors,[14] as in the re-initiation step of chain-transfer catalysis, as well as in hydrogenations and hydroformylations. Norton and co-workers measured an M−H BDE of 57.9 kcal/mol for the vanadium hydride $HV(CO)_4$(dppm) (dppm = $Ph_2PCH_2PPh_2$) and measured a re-initiation rate of $\geq 1.75 \times 10^{-2}$ M^{-1} s^{-1} at 285 K (bottom of Scheme 2).[15] Norton demonstrated a monotonic increase in rates of hydrogen transfer to styrene with decreasing metal hydride bond strengths from 62.2 to 54.9 kcal/mol. $Fe_{(1-x)}S$ catalysts enable selective cleavage of aromatic−alkyl bonds if the aromatic ring is activated by alkyl substitution or is otherwise more reactive (to H-atom addition), as in poly-nuclear aromatic hydrocarbons such as naphthalene.[16] Autrey and co-workers explain the enhanced selectivity for hydro-genolytic cleavage of the p-$CH_3C_6H_4$--$CH_2C_6H_4CH_3$ bond over the methyl−aromatic carbon−carbon bond, p-CH_3--$C_6H_4CH_2C_6H_4CH_3$, during FeS-catalyzed hydrogenolysis by invoking an RRD-like mechanism involving rate-determining reversible transfer of a hydrogen atom from FeS−H groups of heterogeneous FeS catalyst to all positions of the aromatic rings of $(p\text{-}CH_3C_6H_4)_2CH_2$, with hydrogen addition at the methyl and benzyl *ipso* positions of the aromatic structure leading to competing methyl or benzyl scission.[17]

The stepwise homolytic hydrogen transfer to olefins from a hydrogen-containing metal sulfide catalyst (Scheme 1) corresponds directly to the molecule-assisted homolytic transfer of hydrogen between hydrocarbons and olefinic acceptors (Scheme 2, top).[13] The role of M−H bond strengths has been demonstrated for the homolytic reactivity of the Mo−H bond with carbon-centered radicals[19] and for the activation of the bridging

(9) Appel, A. M.; Lee, S.-J.; Franz, J. A.; DuBois, D. L.; Rakowski DuBois, M. *J. Am. Chem. Soc.* **2009**, *131*, 5224–5232.
(10) Wang, H.; Salveson, I. *Phase Transitions* **2005**, *78*, 547–567.
(11) Ades, H. F.; Companion, A. L.; Subbaswamy, K. R. *Energy Fuels* **1994**, *8*, 71–76.
(12) McMillen, D. F.; Malhotra, R.; Chang, S. J.; Ogier, W. C.; Nigenda, S. E.; Fleming, S. H. *Fuel* **1987**, *66*, 1611–1620.
(13) Rüchardt, C.; Gerst, M.; Ebenhoch, J. *Angew. Chem., Int. Ed. Engl.* **1997**, *36*, 1406.
(14) (a) Bullock, R. M.; Samsel, E. G. *J. Am. Chem. Soc.* **1990**, *112*, 6886–6898. (b) Norton, J. R. *Isr. J. Chem.* **1991**, *31*, 55–66.
(15) (a) Choi, J.; Pulling, M. E.; Smith, D. M.; Norton, J. R. *J. Am. Chem. Soc.* **2008**, *130*, 4250–4252. (b) Gridnev, A. A.; Ittel, S. D. *Chem. Rev.* **2001**, *101*, 3611–3659. Heuts, J. P.A.; Roberts, G. E.; Biasutti, J. D. *Aust. J. Chem.* **2002**, *55*, 381–398. (c) Halpern, J. *Pure Appl. Chem.* **1986**, *58*, 575–584. Eisenberg, D. C.; Norton, J. R. *Isr. J. Chem.* **1991**, *31*, 55–66.
(16) (a) Walter, T. D.; Klein, M. *Energy Fuels* **1995**, *9*, 1058–1061. (b) Farcasiu, M.; Smith, C. *Energy Fuels* **1991**, *5*, 83. (c) Huffman, G. P.; Ganguly, B.; Zhao, J.; Rao, K. R. P. M.; Shah, N.; Feng, Z.; Taghiei, M. M.; Lu, F.; Wender, I.; Pradhan, V. R.; Tierney, J. W.; Seehra, M. S.; Ibrahim, M. M.; Shabtai, J.; Eyring, E. M. *Energy Fuels* **1993**, *7*, 285.
(17) Autrey, T.; Linehan, J. C.; Camaioni, D. M.; Kaune, L. E.; Watrob, H. M.; Franz, J. A. *Catal. Today* **1996**, *31*, 105–111.
(18) (a) Choi, J.; Pulling, M. E.; Smith, D. M.; Norton, J. R. *J. Am. Chem. Soc.* **2008**, *130*, 4250–4252. (b) Gridnev, A. A.; Itel, S. D. *Chem. Rev.* **2001**, *101*, 3611–3659. (c) Heuts, J. P. A.; Roberts, G. E.; Biasutti, J. D. *Aust. J. Chem.* **2002**, *55*, 381–398.
(19) Franz, J. A.; Linehan, J. C.; Birnbaum, J. C.; Hicks, K. W.; Alnajjar, M. S. *J. Am. Chem. Soc.* **1999**, *121*, 9824–9830.

Chart 1. Abbreviations and Basic Structures for Iron Sulfide Complexes in This Study

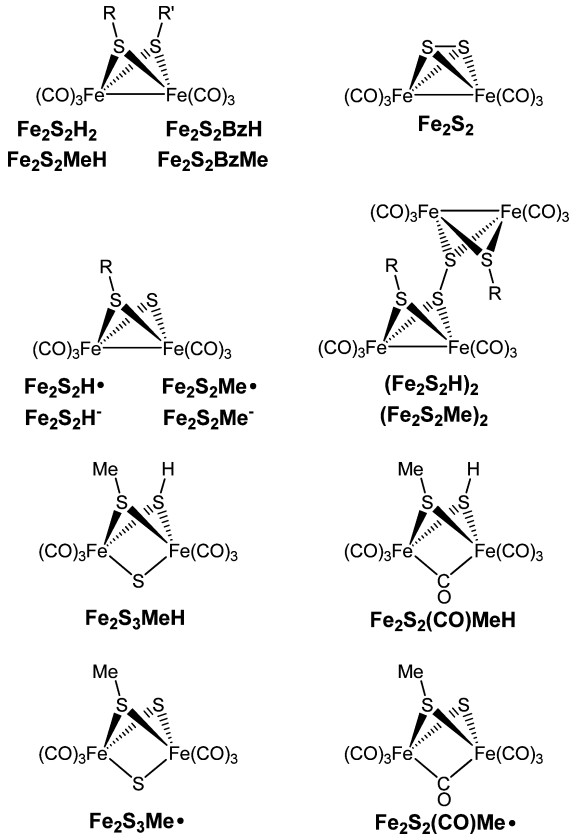

S−H group in the system [CpMo(μ-SH)(μ-S)]$_2$ to reactivity with benzyl radical.[20] The rate of hydrogen abstraction by benzyl radical from the Mo(μ_2-SH)Mo group was found to be a factor of 100 faster than that with alkanethiols. The basis of this rate enhancement, although attenuated by steric effects, was revealed in our recent finding that the S−H BDE in Cp*Mo(μ_2-SH)(μ_2-SCH$_3$)(μ-S)$_2$MoCp* is reduced to 72 kcal/mol compared to those of H_2S (91.2 kcal/mol), simple alkanethiols (87 kcal/mol), and arenethiols (78−79 kcal/mol).[24]

Knowledge of FeS−H bond strengths is essential to understanding the catalytic reactivity of homogeneous and heterogeneous FeS catalysts. We thus present the first measurement of an S−H homolytic bond strength and kinetic homolytic reactivity in a prototype Fe(μ-SH)Fe system. The results provide insight into the reactivity of similar structures expected for heterogeneous pyrite/pyrrhotite catalyst systems. This study examines the homolytic reactivity of the μ_2-SH group in low-valent iron systems (see Chart 1) for hydrogen atom transfer from (OC)$_3$Fe(μ-SH)$_2$Fe(CO)$_3$ (**$Fe_2S_2H_2$**) and (OC)$_3$Fe(μ-SCH$_3$)(μ-SH)$_2$Fe(CO)$_3$ (**Fe_2S_2MeH**) to benzyl radical. DFT calculations are applied to estimate the S−H bond strength of **$Fe_2S_2H_2$** and **Fe_2S_2MeH** for comparison with that of the S−H group of alkane- and arenethiols, and the experimental homolytic solution bond dissociation free energy (SBDFE) of **Fe_2S_2MeH** is presented. The kinetic reactivity of benzyl radical with the μ_2-SH group of the di-iron systems is correlated in a Polanyi relationship with the reactivity predicted from the S−H bond strengths of **$Fe_2S_2H_2$**, **Fe_2S_2MeH**, and a series of thiols, and new absolute

(20) Franz, J. A.; Birnbaum, J. C.; Kolwaite, D. S.; Linehan, J. C.; Camaioni, D. M.; Dupuis, M. *J. Am. Chem. Soc.* **2004**, *126*, 6680–6691.

Chart 2. **Fe_2S_2R** and **Fe_2S_2RH** Isomers in This Study

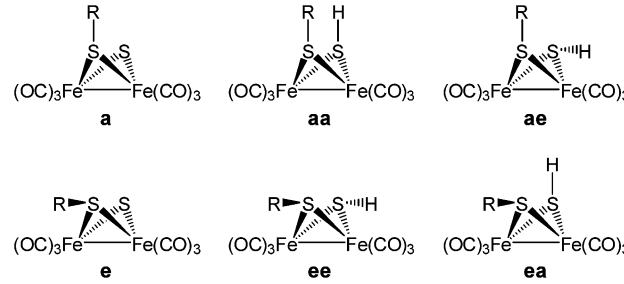

rate expressions for abstraction of a hydrogen atom by benzyl radical from H_2S and thiophenol are described. Finally, the effect on S−H bond strengths of replacing the Fe−Fe bond in the above structures with μ-S or μ-CO bridging structures is examined.

Results and Discussion

Kinetics of Reaction of $Fe_2S_2H_2$ and Fe_2S_2MeH with Benzyl Radical. For hydrogen atom donors possessing a single abstractable hydrogen atom, photolysis in the presence of dibenzyl ketone (DBK) to produce benzyl radical and the subsequent measurement of the resulting toluene and bibenzyl concentrations provide a convenient means of measuring rate constants for hydrogen atom abstraction. Accurate self-termination rate expressions for benzylic and other alkyl radicals in common solvents have proven particularly useful in kinetic determination of competing rate processes.[21,23] Using available[19] values for the self-termination rate of benzyl radical, k_t, in benzene, the rate constant for abstraction is given by eq 1,

$$k_{abs} = -\frac{k_t^{1/2}\ln(1 - [\text{toluene}]/[\text{DH}]_0)}{[\text{bibenzyl}]^{1/2}\Delta t^{1/2}} \qquad (1)$$

where $[DH]_0$ is the initial concentration of the hydrogen atom donor. The steady-state photolysis of DBK produces benzyl and phenylacetyl radicals (eq 2a, Scheme 3), which is followed by rapid decarbonylation of the phenylacetyl radical (eq 2b) to form a second benzyl radical. The generated benzyl radicals abstract hydrogen atoms from donors to produce toluene (eq 3) or self-terminate to produce bibenzyl (eq 4).

Equation 1 accounts for declining donor concentration during photolysis of DBK. The μ_2-SH donor **$Fe_2S_2H_2$** exists as a mixture of three isomers, axial−equatorial (**ae** = **ea**), axial−axial (**aa**), and equatorial−equatorial (**ee**) (Chart 2). When photolysis of DBK and **$Fe_2S_2H_2$** is carried out to sufficient extent of reaction to allow observation of products by NMR, the S−H peaks of the **aa**, **ee**, and **ae** isomers are observed to decrease, with no evidence of new S−H NMR transitions associated with

(21) See, e.g.: (a) Franz, J. A.; Suleman, N. K.; Alnajjar, M. S. *J. Org. Chem.* **1986**, *51*, 19–25. (b) Autrey, S. T.; Alnajjar, M. S.; Nelson, D. A.; Franz, J. A. *J. Org. Chem.* **1991**, *56*, 2197–2202. (c) Alnajjar, M. S.; Franz, J. A. *J. Am. Chem. Soc.* **1992**, *114*, 1052–1058. (d) Franz, J. A.; Linehan, J. C.; Birnbaum, J. C.; Hicks, K. W.; Alnajjar, M. S. *J. Am. Chem. Soc.* **1999**, *121* (42), 9824–9830. (e) Kandanarachchi, P. H.; Autrey, T.; Franz, J. A. *J. Org. Chem.* **2002**, *67*, 7937–7945. (f) Franz, J. A.; Kolwaite, D. S.; Linehan, J. C.; Rosenberg, E. *Organometallics* **2004**, *23*, 441–445.

(22) von Smoluchowski, M. Z. *Z. Phys. Chem. Stoechiom. Verwandtsschaftl.* **1917**, *92*, 129.

(23) Fischer, H.; Paul, H. *Acc. Chem. Res.* **1987**, *20*, 200–206.

(24) Appel, A. M.; Lee, S.-J.; Franz, J. A.; DuBois, D. L.; DuBois, M. R.; Birnbaum, J. C.; Twamley, B. *J. Am. Chem. Soc.* **2008**, *130*, 8940–8951.

Scheme 3. Hydrogen Atom Abstraction from $Fe_2S_2H_2$ by Benzyl Radical

$$PhCH_2COCH_2Ph \xrightarrow[>330nm]{h\nu} PhCH_2\dot{C}O + PhCH_2^{\bullet} \quad (2a)$$

$$PhCH_2\dot{C}O \xrightarrow{k_{sc}} PhCH_2^{\bullet} + CO \quad (2b)$$

$$PhCH_2^{\bullet} + Fe_2S_2H_2 \xrightarrow{k_{abs}} PhCH_3 + Fe_2S_2H^{\bullet} \quad (3)$$

$$2\,PhCH_2^{\bullet} \xrightarrow{k_t} PhCH_2CH_2Ph \quad (4)$$

$$PhCH_2^{\bullet} + Fe_2S_2H^{\bullet} \xrightarrow{k_{ct,disp}} PhCH_3 + Fe_2S_2 \quad (5)$$

$$PhCH_2^{\bullet} + Fe_2S_2H^{\bullet} \xrightarrow{k_{ct,comb}} Fe_2S_2BzH \quad (6)$$

$$2\,Fe_2S_2H^{\bullet} \xrightarrow{k'_{disp}} Fe_2S_2H_2 + Fe_2S_2 \quad (7)$$

$$2\,Fe_2S_2H^{\bullet} \xrightarrow{k_{dim}} (Fe_2S_2H)_2 \quad (8)$$

cross-combination product Fe_2S_2BzH (eq 6) or self-termination product $(Fe_2S_2H)_2$ (eq 8). The termination pathways of $Fe_2S_2H^{\bullet}$ are thus defined to be cross-disproportionation with benzyl radical to form toluene and Fe_2S_2 (eq 5) and self-disproportionation of two $Fe_2S_2H^{\bullet}$ radicals to form $Fe_2S_2H_2$ and Fe_2S_2 (eq 7). Determination of the ratio of yields of toluene formed in the primary reaction step (eq 3) versus cross-disproportionation (eq 5) is made possible by the lack of formation of the cross-combination product (Fe_2S_2BzH, eq 6), as described in the Experimental Procedures. Thus, all benzyl radical-derived products appear as toluene and bibenzyl. This allows numerical integration of eqs 2, 3, 4, 5, and 7, with k_{abs} varied to reproduce yields of toluene and bibenzyl. The numerical integration requires values of k_t (eq 4), $k_{ct,disp}$ (eq 5), and k'_{disp} (eq 7). Since only disproportionation appears to occur in reaction of $Fe_2S_2H^{\bullet}$ with benzyl radical (eq 5) or in self-reaction (eq 7), the total diffusion-controlled encounter rates, modified by singlet radical pair spin selection, can be assigned to these processes. The total self-termination rate of $Fe_2S_2H^{\bullet}$ is calculated from the modified von Smoluchowski equation[22] using experimental diffusion coefficients of Fe_2S_2 as a model for $Fe_2S_2H^{\bullet}$. The estimation of diffusion- and spin-selected self- and cross-reaction of reactive free radicals (see Experimental Procedures for details) is facilitated by the narrow total range of self-reaction rates exhibited by small free radicals in nonassociating solvents, ca. $(1-8) \times 10^9\ M^{-1}\ s^{-1}$, at the temperatures employed here, unless the approach of the radical centers is specifically hindered by bulky substituents.[23] The self-termination rate of $Fe_2S_2H^{\bullet}$ will be expected to be to comparable to that of small alkyl radicals and predictable from the viscosity of the solvent and the reaction distances (see Experimental Procedures for details). Molecular modeling reveals the bridging sulfide and hydrosulfide in $Fe_2S_2H^{\bullet}$ to be sterically unencumbered and readily accessible. This is in contrast to, for example, slowly dimerizing molybdenum- ($Cp^*Mo(\mu\text{-}SCH_3)(\mu\text{-}S^{\bullet})MoCp^*$)[24] or chromium-centered radicals ($(CO)_3Cr^{\bullet}$),[25] where steric hindrance results in self-termination rates of 6.5×10^7 and $2.7 \times 10^8\ M^{-1}\ s^{-1}$ for the Mo and Cr radicals, respectively, slower by factors of 30 and 10 than diffusion-controlled rates, clearly due to front strain in forming S−S and Cr−Cr bonds for these species.

(25) Yao, Q.; Bakac, A.; Espenson, J. H. *Organometallics* **1993**, *12*, 2010–2012.

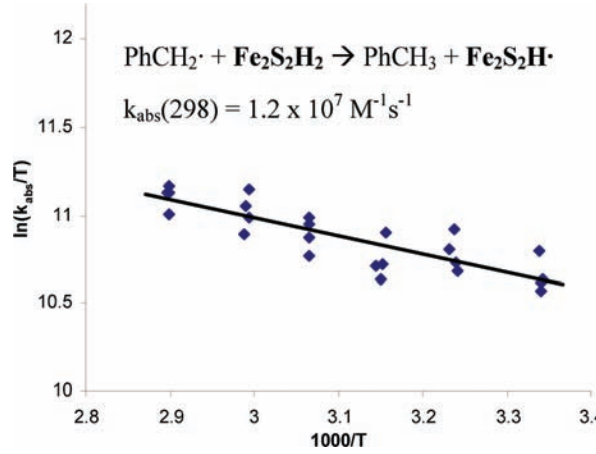

Figure 1. Eyring plot of temperature-dependent rate data for abstraction of a hydrogen atom by benzyl radical from $Fe_2S_2H_2$ in benzene. Rate constants are per abstractable hydrogen atom.

$Fe_2S_2H^{\bullet}$ is predicted to self-terminate, assuming no steric retardation, at a rate constant of $2.04 \times 10^9\ M^{-1}\ s^{-1}$, based on experimental diffusion constants measured for Fe_2S_2. The assumption of the absence of steric retardation is supported by the known formation of stable dimers of the radical $Fe_2S_2R^{\bullet}$ (R = Ph). The resulting temperature-dependent rate constants from numerical integration of eqs 2−5 and 7 for reaction of benzyl radical with $Fe_2S_2H_2$ are depicted in Figure 1 and tabulated in Table 1.

The methylated derivative, Fe_2S_2MeH, was prepared in order to avoid the ambiguity created by the presence of two hydrosulfides in $Fe_2S_2H_2$. For Fe_2S_2MeH, only one hydrosulfide is present, and so abstracted hydrogen atoms have only one source, thereby eliminating the need for eqs 5 and 7. Equations 9, 10, and 11 (Scheme 4) describe reactions that occur as a result of steady-state photolysis of DBK in the presence of isomers of Fe_2S_2MeH, with benzyl radical formation and self-termination described above in eqs 2a, 2b, and 4. Formation of toluene occurs only in the abstraction step (eq 9); thus, measurement of toluene and bibenzyl provides the abstraction rate constant, k_{abs}, using eq 1. Cross-termination product Fe_2S_2MeBz (eq 10) and self-termination product $(Fe_2S_2Me)_2$ (eq 11) are known structures. Kinetic data are depicted in Figure 2 and tabulated in Table 1. Because methyl substitution eliminates cross-disproportionation for Fe_2S_2MeH, because $Fe_2S_2H_2$ was found to decompose over several days, and because of the need to model cross-termination and self-termination of the Fe_2S_2MH radical, we regard the rate constants for Fe_2S_2MeH as inherently more reliable. This is also reflected in the statistical errors in rate constants, as the error for $Fe_2S_2H_2$ is approximately twice that for Fe_2S_2MeH.

Scheme 4. Hydrogen Atom Abstraction from Fe_2S_2MeH by Benzyl Radical

$$PhCH_2^{\bullet} + Fe_2S_2MeH \xrightarrow{k_{abs}} PhCH_3 + Fe_2S_2Me^{\bullet} \quad (9)$$

$$PhCH_2^{\bullet} + Fe_2S_2Me^{\bullet} \xrightarrow{k_{ct,comb}} Fe_2S_2MeBz \quad (10)$$

$$2\,Fe_2S_2Me^{\bullet} \xrightarrow{k_{dim}} (Fe_2S_2Me)_2 \quad (11)$$

Kinetics of Reaction of Benzyl and H_2S. The reactions of benzyl radical with H_2S in benzene under steady-state photolysis

Table 1. Rate Expressions for the Reaction of Benzyl Radical with the μ-SH Hydrogen Atom in **$Fe_2S_2H_2$**, **Fe_2S_2MeH**, a Mo(μ-SH)Mo Complex, and Thiols[a]

hydrogen donor	XS−H BDE (kcal/mol)	log A (M^{-1} s^{-1})[f]	$\Delta S^{\ddagger}$ (eu) (T_m, K)[f]	E_a (kcal/mol)[f]	$\Delta H^{\ddagger}$ (kcal/mol)[f]	k (M^{-1} s^{-1}/H) (298 K)	T_m (K_[h]	temp range (K)
Fe_2S_2MeH	74.2 (exp) 73.2 (calc)[b]	9.29 ± 0.16	−18.1 ± 0.8	2.60 ± 0.23	1.97 ± 0.23	(2.4 ± 0.23) × 10^7	316	293−344
$Fe_2S_2H_2$	73.1 (calc)[b] 73.2 (calc)[b,c]	9.04 ± 0.19	−19.3 ± 0.8	2.66 ± 0.28	2.03 ± 0.28	(1.2 ± 0.49) × 10^7	322	299−345
[CpMo(μ-S)(μ-SH)]$_2$	70.6 ± 2.2 (expt)[g] 73.2 (calc)	9.07 ± 0.19	−19.2 ± 0.9	3.62 ± 0.29	2.96 ± 0.29	(2.7 ± 0.35) × 10^6	331	295−372
C_6H_5SH	79.1[d]	8.52 ± 0.015	−21.7 ± 0.6	4.27 ± 0.22	3.62 ± 0.22	(2.5 ± 0.33) × 10^5	335	298−366
$CH_3(CH_2)_7SH$[c]	87.3[d,e]	7.89 ± 0.18	−24.7 ± 0.8	4.64 ± 0.27	3.96 ± 0.27	(3.1 ± 0.37) × 10^4	341	295−374
H_2S	91.2[e]	7.85 ± 0.34	−24.8 ± 0.8	5.77 ± 0.49	5.13 ± 0.50	(4.2 ± 0.51) × 10^3	321	293−348

[a] Errors are 1σ. Rate constants are reported per abstractable hydrogen atom, k (M^{-1} s^{-1})/H. [b] From DFT calculations, this work, see text. [c] Reference 20. [d] Bordwell, F. G.; Zhang, X.-M.; Satish, A. V.; Cheng, J. P. *J. Am. Chem. Soc.* **1994**, *116*, 6605. [e] Nicovich, J. M.; Kreutter, K. D.; van Dijk, C. A.; Wine, P. A. *J. Phys. Chem.* **1992**, *96*, 2518. [f] A, Arrhenius pre-exponential factor; E_a, Arrhenius exponential constant in $k = A\ e^{-E_a/RT}$; $\Delta S^{\ddagger} = -R(\ln(k_{T_m}/T_m) - \ln(k_b/h) + \Delta H^{\ddagger}/RT_m)$; $\Delta H^{\circ} = -R(\partial \ln(k_{abs}/T)/\partial(1/T))$; h, Planck's constant, 6.6260755^{-34} J s; and k_b, Boltzmann's constant, 1.380658 × 10^{-23} J K^{-1}. [g] Reference 9. [h] T_m, mean temperature of kinetic experiments.

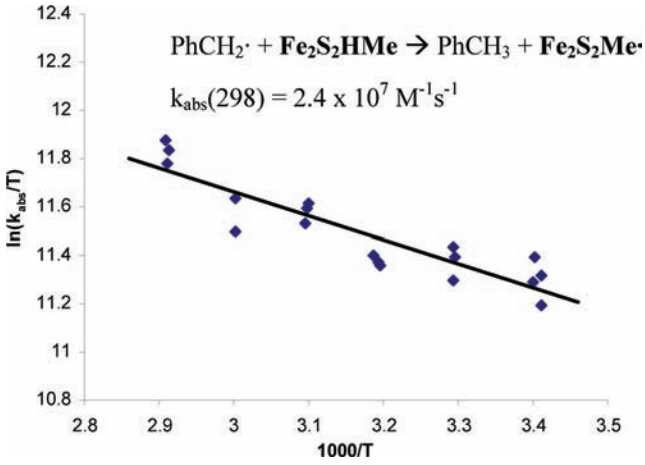

Figure 2. Eyring plot of temperature-dependent rate data for abstraction of a hydrogen atom by benzyl radical from **Fe_2S_2MeH** in benzene.

of DBK are presented in eqs 13−18 (Scheme 5), with benzyl radical formation and self-termination described above in eqs 2a, 2b, and 4. Toluene is formed by reaction of benzyl radical with H_2S (eq 13). However, if photolysis is continued beyond a short extent of conversion of H_2S (ca. 0.1%), toluene may be formed by reaction with HSSH (eq 16). Taking the S−H BDE of HSSH to be 73.6 kcal/mol—from among the choices of an older experimental value, 70.0 ± 1.5 kcal/mol,[26] an older computed value of 73.2 kcal/mol,[27] and a recent state-of-the-art calculation, 73.6 kcal/mol[28]—the reaction of benzyl radical with HSSH is predicted to be quite fast, 1.3 × 10^7 M^{-1} s^{-1}, on the basis of the Polanyi expression developed here for abstraction by benzyl radical from thiols, $\ln(k_{abs}/M^{-1}\ s^{-1}, 298\ K) = -0.465\Delta H^{\circ} + 50.64$ (see discussion below). At H_2S concentrations of ca. 0.1 M with $k_{abs} = 4 \times 10^3$ M^{-1} s^{-1}, concentrations of HSSH would not have accumulated to greater than about 10^{-4} M, preventing HSSH from contributing significantly to the observed toluene.

$PhCH_2SH$, formed by cross-termination in eq 14, was observed at low but detectable concentrations. However, this hydrogen atom donor will react with benzyl radical (eq 17) with a rate constant of only about 3 × 10^4 M^{-1} s^{-1}, thereby contributing insignificantly to the observed toluene due to both its low concentration and its low abstraction rate. The production of trace quantities of $PhCH_2SCH_2Ph$ indicates the operation of eqs 17 and 18. The reaction of $HS^{\bullet}$ with $PhCH_2SH$ ($\Delta H^{\circ} = -4$ kcal/mol) is expected to occur with rate constants in the range 10^4−10^5 M^{-1} s^{-1}, from comparison of rate constants for hydrogen atom transfer between hexanethiyl radical and octanethiol ($\Delta H^{\circ} = 0$ kcal/mol, $k_{abs}(298\ K) = 2.7 \times 10^4$ M^{-1} s^{-1}) and between thiophenol and octanethiyl radical ($\Delta H^{\circ} = -7$ kcal/mol, $k_{abs}(298\ K) = 1.3 \times 10^5$ M^{-1} s^{-1}).[29] The detection of only trace quantities of the second-generation products is consistent with toluene being produced nearly exclusively in eq 13. From the temperature-dependent rate data for hydrogen abstraction by benzyl from H_2S, $\Delta H^{\ddagger} = 5.13 \pm 0.99$ kcal/mol and $\Delta S^{\ddagger} = -24.8 \pm 3.2$ cal/(mol K), giving $k_{abs} = 4.2 \times 10^3$ M^{-1} s^{-1} at 25 °C. This rate constant is about 100-fold slower than that for thiophenol, yielding correspondingly greater magnitudes of $\Delta S^{\ddagger}$ and $\Delta H^{\ddagger}$, fully consistent with expected trends in conventional bimolecular rate parameters for hydrogen transfer between carbon and heteroatom centers.

Kinetics of Reaction of Benzyl Radical with Thiophenol. Temperature-dependent rate data were previously determined[30] for the reaction of benzyl radical with thiophenol in *hexane*: $\Delta H^{\ddagger} = 3.13 \pm 0.14$ kcal/mol and $\Delta S^{\ddagger} = -22.8 \pm 1.1$ cal/(mol K), giving $k_{abs} = 3.1 \times 10^5$ M^{-1} s^{-1} at 25 °C. In this work, rate constants were determined for reaction of benzyl radical with thiophenol in *benzene*. The kinetic scheme is directly analogous to that for the reaction of benzyl radical and **Fe_2S_2MeH**, and eq 1 applies. From the temperature-dependent rate data for hydrogen abstraction by benzyl from thiophenol in benzene, $\Delta H^{\ddagger} = 3.62 \pm 0.43$ kcal/mol and $\Delta S^{\ddagger} = -21.7 \pm 1.3$ cal/(mol K), giving $k_{abs} = 2.5 \times 10^5$ M^{-1} s^{-1} at 25 °C. These activation parameters agree within experimental error with the earlier hexane values.

Experimental Determination of the S−H Bond Dissociation Free Energy of Fe_2S_2MeH. The homolytic solution bond dissociation free energy (SBDFE) of **Fe_2S_2MeH** was determined by using a combination of cyclic voltammetry and pK_a measurements in acetonitrile. The pK_a of **Fe_2S_2MeH** was determined to be 16.0 ± 0.4 by equilibration with 2,4,6-trimethylpyridine (pK_a = 14.98),[31] as measured using ^{1}H NMR.

(26) McMillen, D. F.; Golden, D. M. *Annu. Rev. Phys. Chem.* **1982**, *33*, 493.
(27) DiLabio, G. A.; Pratt, D. A.; LoFaro, A. D.; Wright, J. S. *J. Phys. Chem.* **1999**, *103*, 1653–1661.
(28) Grant, D. J.; Dixon, D. A.; Francisco, J. F.; Feller, D.; Peterson, K. A. *J. Phys. Chem. A.* **2009**, submitted.
(29) Alnajjar, M. S.; Garrossian, M. S.; Autrey, S.T. ; Ferris, K. F.; Franz, J. A. *J. Phys. Chem.* **1992**, *96*, 7037–7043.
(30) Franz, J. A.; Suleman, N. K.; Alnajjar, M. S. *J. Org. Chem.* **1986**, *51*, 19.
(31) Kaljurand, I.; Kutt, A.; Soovali, L.; Rodima, T.; Maemets, V.; Leito, I.; Koppel, I. A. *J. Org. Chem.* **2005**, *70*, 1019–1028.

Cyclic voltammetry (CV) in acetonitrile revealed an irreversible oxidation wave for the anion, $\mathbf{Fe_2S_2Me^-}$, for scan rates from 0.05 to 100 V/s. The cause of this irreversibility is assigned to rapid dimerization of $\mathbf{Fe_2S_2Me^\bullet}$ to form $\mathbf{(Fe_2S_2Me)_2}$, supported by the known dimer formation in the phenyl analogue.[32] Assuming a diffusion- and spin-selected self-termination rate (2×10^9 M^{-1} s^{-1}), $E_{1/2}$ can be estimated from the irreversible peak potentials at each scan rate by use of CV simulations (DigiSim).[33] Using the corrected potentials for each of the scan rates, $E_{1/2}$ was estimated to be -0.26 ± 0.05 V vs ferrocene. By combining the pK_a and $E_{1/2}$ using eq 12, the homolytic S−H SBDFE for $\mathbf{Fe_2S_2MeH}$ was determined to be 69.4 ± 1.7 kcal/mol in acetonitrile, corresponding to a gas-phase BDE of 74.2 kcal/mol.[34,35]

$$\text{SBDFE} = 23.06E_{1/2} + 1.37\text{p}K_a + 53.6 \qquad (12)$$

Scheme 5. Hydrogen Atom Abstraction from H_2S by Benzyl Radical

$$PhCH_2^\bullet + H_2S \xrightarrow{k_{abs}} PhCH_3 + HS^\bullet \qquad (13)$$

$$PhCH_2^\bullet + HS^\bullet \xrightarrow{k_{ct}} PhCH_2SH \qquad (14)$$

$$2\,HS^\bullet \xrightarrow{k_t'} HSSH \qquad (15)$$

$$PhCH_2^\bullet + HSSH \xrightarrow{k_{abs}'} PhCH_3 + HSS^\bullet \qquad (16)$$

$$PhCH_2SH + R^\bullet \longrightarrow PhCH_2S^\bullet + RH \quad (R = HS, PhCH_2) \qquad (17)$$

$$PhCH_2S^\bullet + PhCH_2 \xrightarrow{k_{ct}'} PhCH_2SCH_2Ph \qquad (18)$$

Computational Studies. Electronic structure calculations (using DFT and TDDFT methods) have been recently reported for $Fe_2(S_2C_3H_6)(CO)_6$, an analogue of the **aa** isomer of $\mathbf{Fe_2S_2H_2}$ in which the S−H groups have been replaced by a bridging propanedithiolate, $SCH_2CH_2CH_2S$.[36] Earlier work characterized the molecular orbitals of Fe_2S_2 and Fe_2S_2.[37] Recently, Silaghi-Dumitrescu, Bitterwolf, and King examined the electronic structures, geometries, and excited states of Fe_2S_2 and the diradicals derived from Fe_2S_2 and related phosphorus analogues.[38] Thus, the ground and excited states of the parent Fe_2S_2 cluster and of the diradicals have been characterized, but not those of the related radical systems.

In the current work, electronic structure calculations were carried out using Gaussian 03.[39] Geometries, frequencies, and electronic energies were determined using DFT in the restricted open-shell reference, ROB3LYP,[40] for radicals and RB3LYP

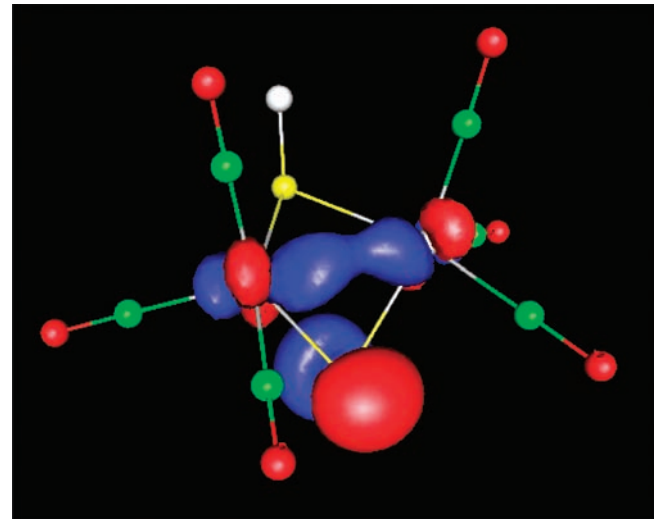

Figure 3. Alpha orbital density of the SOMO of $\mathbf{Fe_2S_2H^\bullet}$. Spin density is primarily located about the two Fe atoms and the bridging S atoms.

for parent thiols with the CEP-121G basis set and ECP pseudopotential for Fe and the 6-311++G(2d,2p) basis set for C, H, S, and O atoms.[41] Ground states were confirmed by the absence of imaginary frequencies. Tight SCF convergence criteria were used. Vibrational frequencies were left unscaled in the enthalpy and free energy calculations, as their application leads to less than 0.2 kcal/mol difference in energies for the small scaling factors of DFT methods. The performance and shortcomings of B3LYP have been reviewed for organic molecules.[42] Truhlar and co-workers have compared B3LYP with more recently developed approaches for metallic compounds.[43] The prediction of organic S−H bond strengths is quite satisfactory with B3LYP at the level of theory used here. The present work provides a comparison of experimental data with results of the B3LYP and ECP density functional methods for organometallic S−H bond strengths.

The orbital spin density of the SOMO of $\mathbf{Fe_2S_2H^\bullet}$ is depicted in Figure 3. Geometries of $\mathbf{Fe_2S_2MeH}$ (**ae**) and of the radical $\mathbf{Fe_2S_2Me^\bullet}$ are depicted in Figure 4 and Table 2. The butterfly geometry of the parent structures $\mathbf{Fe_2S_2MeH}$ and $\mathbf{Fe_2S_2H_2}$ is retained in the product radicals $\mathbf{Fe_2S_2Me^\bullet}$ and $\mathbf{Fe_2S_2H^\bullet}$, but with extension and weakening of the Fe−Fe bond. Electron spin densities for $\mathbf{Fe_2S_2Me^\bullet}$ and $\mathbf{Fe_2S_2H^\bullet}$ are largely shared between the two iron centers and the bridging μ-S bridge.

DFT bond lengths calculated by the method used here typically give bond lengths 0−3% longer than X-ray crystal structure bond lengths. This is illustrated in Table 3, which presents X-ray data for $\mathbf{Fe_2S_2Et_2}$[44] and $\mathbf{Fe_2S_2}$[45] (Figure 5) to compare with geometric parameters obtained using the B3LYP functional and CEP-121G on Fe and 6-311++G(2d,2p) on C,

(32) Seyferth, D.; Kiwan, A. M.; Sinn, E. *J. Organomet. Chem.* **1985**, *281*, 111–118.
(33) Rudolph, M.; Feldberg, S. W. *DigiSim*, version 3.03b; Bioanalytical Systems. 2004.
(34) Wayner, D. D. M.; Parker, V. D. *Acc. Chem. Res.* **1993**, *26*, 287–294.
(35) Ellis, W. W.; Raebiger, J. W.; Curtis, C. J.; Bruno, J. W.; DuBois, D. L. *J. Am. Chem. Soc.* **2004**, *126*, 2738–2743.
(36) Bertini, L.; Greco, C.; De Gioia, L.; Fantucci, P. *J. Phys. Chem. A* **2009**, *113*, 5657–5670.
(37) DeKock, R. L.; Baerends, E. J.; Hengelmolen, R. *Organometallics* **1984**, *3*, 289–292.
(38) Silaghi-Dumitrescu, I.; Bitterwolf, T. E.; King, R. B. *J. Am. Chem. Soc.* **2006**, *128*, 5342–5343.
(39) Frisch, M. J.; et al. *Gaussian 03*, Revision D.02; Gaussian, Inc.: Wallingford, CT, 2004.
(40) (a) Becke, A. D. *J. Chem. Phys.* **1993**, *98*, 5648. (b) Lee, C.; Yang, W.; Parr, R. G. *Phys. Rev.* **1988**, *B37*, 785.
(41) (a) Krishnan, R.; Binkley, J. S.; Seeger, R.; Pople, J. A. *J. Chem. Phys.* **1980**, *72*, 650. (b) Blaudeau, J.-P.; McGrath, M. P.; Curtiss, L. A.; Radom, L. J. *Chem. Phys.* **1997**, *107*, 5016. (c) Clark, T.; Chandrasekhar, J.; Schleyer, P. v. R. *J. Comput. Chem.* **1983**, *4*, 294.
(42) Tirado-Rives, J.; Jorgensen, W. L. *J. Chem. Theory Comput.* **2008**, *4*, 297–306.
(43) Zhao, Y.; Schultz, N. E.; Truhlar, D. G. *J. Chem. Phys.* **2005**, *123*, 161103.
(44) Seyferth, D.; Kiwan, A. M. *J. Organomet. Chem.* **1985**, *281*, 111–118.
(45) Wei, C. H.; Dahl, L. F. *Inorg. Chem.* **1965**, *4*, 1–11.

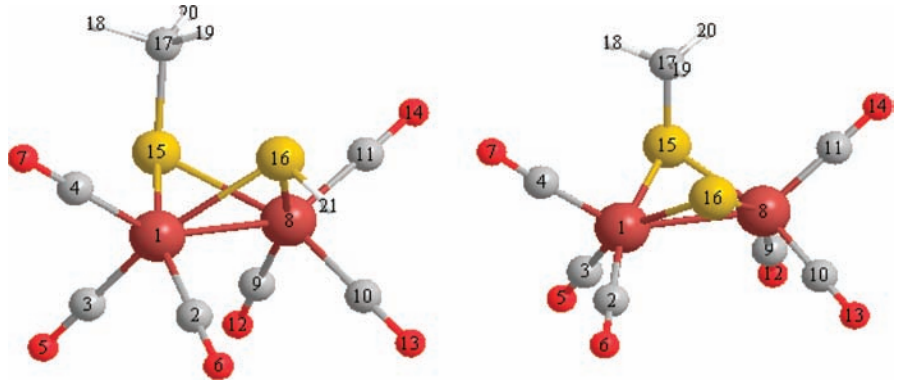

Figure 4. DFT butterfly geometries of (left) **Fe_2S_2MeH** (**ae**) and (right) **$Fe_2S_2Me^{\bullet}$** (**a**).

Table 2. DFT Geometries of **Fe_2S_2MeH** (**ae**) and **$Fe_2S_2Me^{\bullet}$** (**a**)[a]

	Fe_2S_2MeH (ae)	$Fe_2S_2Me^{\bullet}$ (a)
	Bond Distances, Å	
Fe(1)−Fe(8)	2.53	2.66
Fe(8)−S(15)	2.31	2.32
Fe(1)−S(16)	2.32	2.23
Fe(8)−C(9)	1.808	1.834
Fe(8)−C(10)	1.805	1.82
Fe(8)−C(11)	1.809	1.806
S(15)−C(17)	1.838	1.834
S(16)−H(21)	1.345	
	Angles, deg	
Fe(1)−S(16)−Fe(8)	66.38	72.99
Fe(1)−S(15)−Fe(8)	65.98	70
Fe(1)−Fe(8)−C(10)	101.76	110.46
C(17)−S(15)−Fe(1)	113.23	109.47
C(9)−Fe(8)−C(10)	92.18	93.92
C(10)−Fe(8)−C(11)	100.22	97.06

[a] See Figure 4.

Table 3. DFT Geometries of **$Fe_2S_2Et_2$** (**ae**) and **Fe_2S_2**[a]

	$Fe_2S_2Et_2$ (ae)	
	length (Å) or angle (°)	
	X-ray[23]	DFT
Fe(1)−Fe(8)	2.537(10)	2.522
Fe(1)−S(15)	2.259(7)	2.315
S(15)−C(17)	1.81(3)	1.854
Fe(1)−S(15)−Fe(8)	68.3(3)	65.916
S(15)−Fe(1)−S(16)	81.0(3)	81.22

	Fe_2S_2	
	length (Å) or angle (°)	
	X-ray[24]	DFT
Fe(1)−Fe(8)	2.552(2)	2.574
Fe(1)−S(15)	2.228(2)	2.284
S(15)−C(16)	2.007(5)	2.073
Fe(1)−S(15)−Fe(8)	69.9(1)	68.6
S(15)−Fe(1)−S(16)	53.5(1)	53.96

[a] See Figure 5.

H, S, and O atoms. The largest discrepancy appears with the S−S bond of **Fe_2S_2**, overestimated by 0.066 Å.

The relative stabilities of **ae**, **ea**, **aa**, and **ee** isomers of FeS clusters were determined using free energy calculations, and the isomers were assigned using GIAO theory in Gaussian03, as described below.[46] The electronic energies, and enthalpy and free energy corrections, for the species of interest are presented in Table 4 (hartree/molecule = 627.5095 kcal/mol). For the three isomers of $(OC)_3Fe(\mu\text{-}SH)_2Fe(CO)_3$, the relative free energies compared to the **ae** (= **ea**) isomer are shown in Chart 3. Using the free energy values from Table 4, the equilibrium ratio **$Fe_2S_2H_2$** (**ae** = **ea**):**$Fe_2S_2H_2$** (**ee**):**$Fe_2S_2H_2$** (**aa**) is calculated to be 1.0:0.21:0.13 in the gas phase. Experimentally, the ratio is found to be 1.0:0.29:0.31 in benzene-d_6 and 1.0: 0.09: 0.1 in $CDCl_3$. Seyferth et al. reported a ratio of **ae**:**ee**:**aa** of 14:2:1.[47] To match the experimental isomer populations observed by NMR with the correct isomers, gauge-independent atomic orbital NMR calculations were carried out with the same level of DFT theory and basis functions utilized for energy calculations. Isotropic chemical shifts were found to be σ_{iso} = 35.0714 and 33.1963 ppm for **$Fe_2S_2H_2$** (**ae**), σ_{iso} = 35.450 ppm for **$Fe_2S_2H_2$** (**aa**), and σ_{iso} = 33.7467 ppm for **$Fe_2S_2H_2$** (**ee**), compared to σ_{iso} = 31.6022 ppm for methane. Using 0.18 ppm for the methane ^{1}H shift reference predicts the equatorial and axial protons of **$Fe_2S_2H_2$** (**ae**) to appear at −1.77 and −3.65 ppm, respectively, corresponding to experimental chemical shifts of equal intensity peaks at −0.61 and −2.85 ppm in benzene-d_6. Similarly, the equatorial protons of **$Fe_2S_2H_2$** (**ee**) and axial protons of **$Fe_2S_2H_2$** (**aa**) are calculated to appear at −2.33 and −4.03 ppm, respectively, corresponding to experimental chemical shifts of −1.134 and −3.20 ppm in benzene-d_6. The calculations consistently show the equatorial protons to be downfield from the axial protons for all isomers. The GIAO NMR calculations, while exhibiting an absolute error of about −1 ppm, correctly predict the ranking of SH chemical shifts and allow the identity of the isomers to be established.

The calculations of the (gas-phase) relative populations of the isomers of **$Fe_2S_2H_2$** from theoretical free energies are much closer to the (solution, benzene-d_6) experimental populations observed in this work than to the populations reported by Seyferth and co-workers. However, it is not known whether the isomers are at equilibrium in solution in Seyferth's early report. Chen et al. reported that **ea**, **ae**, and **ee** isomers of unsymmetric dialkyl derivatives of the iron complexes (e.g., **Fe_2S_2RR'**) are observed and do equilibrate to a constant ratio, with the exception of the **aa** isomer, which is not observed.[48] For the S−H-containing complexes, acid- or base-catalyzed

(46) (a) London, F. *J. Phys. Radium* **1937**, *8*, 397. (b) McWeeny, R *Phys. Rev.* **1962**, *126*, 1028. (c) Ditchfield, R. *Mol. Phys.* **1974**, *27*, 789. (d) Dodds, J. L.; McWeeny, R.; Sadlej, A. J. *Mol. Phys.* **1980**, *41*, 1419. (e) Wolinski, K.; Hilton, J. F.; Pulay, P. *J. Am. Chem. Soc.* **1990**, *112*, 8251.

(47) Seyferth, D.; Henderson, R. S.; Song, L. *J. Organomet. Chem.* **1980**, *192*, C1–C5.

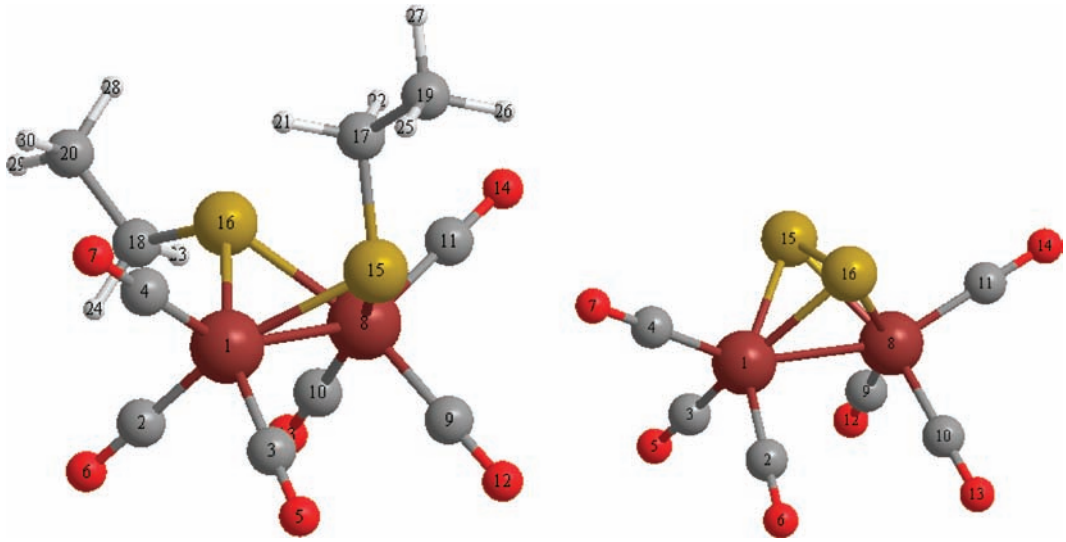

Figure 5. Optimized geometries for (left) **$Fe_2S_2Et_2$** (**ae**) and (right) **Fe_2S_2**.

Table 4. Electronic Energies and Enthalpy Corrections (298 K) for Fe_2S_2 Cluster Systems **$Fe_2S_2H_2$** and **Fe_2S_2MeH** and Radicals **$Fe_2S_2H^{\bullet}$** and **$Fe_2S_2Me^{\bullet}$** (hartree/molecule = 627.5095 kcal/mol)

species	electronic energy (hartree/molecule)	enthalpy [free energy] correction (hartree/molecule)
Fe_2S_2	−1723.37532	0.075547
$Fe_2S_2H_2$ (**ae** = **ea**)	−1724.73186	0.093783[0.024199]
$Fe_2S_2H_2$ (**aa**)	−1724.72968	0.093677[0.023970]
$Fe_2S_2H_2$ (**ee**)	−1724.73019	0.093718[0.024021]
$Fe_2S_2H^{\bullet}$ (**a**)	−1724.10645	0.084343[0.013710]
$Fe_2S_2H^{\bullet}$ (**e**)	−1724.10843	0.084473[0.013944]
Fe_2S_2MeH (**ae**)	−1764.05411	0.124785[0.051375]
Fe_2S_2MeH (**aa**)	−1764.0501139	0.124654[0.050852]
Fe_2S_2MeH (**ea**)	−1764.055151	0.124718[0.051336]
Fe_2S_2MeH (**ee**)	−1764.052825	0.124762[0.051321]
Fe_2S_2Me• (**a**)	−1763.43009	0.115280[0.040752]
$Fe_2S_2Me^{\bullet}$ (**e**)	−1763.43172	0.115281[0.040760]
Fe_2S_3MeH (**ae**)	−2162.29137	0.128037[0.052042]
$Fe_2S_3Me^{\bullet}$ (**a**)	−2161.66861 (UB3LYP, $\langle S^2 \rangle = 0.757$)	0.118969[0.042669]
	−2161.66734 (ROB3LYP)	0.118979[0.042698]
$Fe_2S_2(CO)MeH$ (**ae**)	−1877.39713	0.134666[0.056249]
$Fe_2S_2(CO)Me^{\bullet}$ (**a**)	−1876.78469 (UB3LYP, $\langle S^2 \rangle = 0.799$)	0.125423[0.047232]
	−1876.78477 (ROB3LYP)	0.125510[0.047402]
$H^{\bullet}$	−0.49982 (−0.5)	0.00236

protonation/deprotonation of the S−H protons is expected to lead to more rapid equilibration. For the four isomers of $(OC)_3Fe(\mu\text{-}SH)(\mu\text{-}SCH_3)Fe(CO)_3$, the gas-phase equilibrium ratio is calculated to be 1:0.32:0.09:0.01 for **Fe_2S_2MeH** (**ea**):**Fe_2S_2MeH** (**ae**):**Fe_2S_2MeH** (**ee**):**Fe_2S_2MeH** (**aa**). The solution (benzene-d_6) ratio measured was **Fe_2S_2MeH** (**ea**):**Fe_2S_2MeH** (**ae**) in the ratio 1.0:0.20, while the **ee** and **aa** isomers were not observed. The predicted gas-phase ratios are in reasonable agreement with the solution values, consistent with equivalent free energies of solvation of the various isomers.

Effect of Substitution of μ-S and μ-CO Bridges for the Fe−Fe Bond on SH Bond Strengths. To further address the question of the importance of the Fe−Fe bond in stabilization of the radical on the FeS cluster, we examined the effect of replacing the Fe−Fe bond with μ-S and μ-CO bridges. The latter structure is a familiar feature of part of the core structure of hydrogenase model systems. The H-cluster of FeFe hydrogenases contains an Fe_4S_4 cubane active site bridged to an Fe_2S_2 binuclear cluster, the latter of which contains a CO bridge between two Fe atoms,[49] reminiscent of the complexes studied here. The geometries are found in Tables 6 and 7 and Figures 6 and 7, and the resulting BDEs are shown in Table 5. Replacement of the Fe−Fe bond with the μ-S bond has no effect on the S−H BDE compared to that of the **Fe_2S_2MeH** system. However, insertion of the μ-CO bridge forces a contraction of the Fe−Fe internuclear distance, as well as Fe−C−Fe and Fe−S−Fe angles, in the radical compared to the thiol, resulting in a substantial reduction in BDE from 74 to 66 kcal/mol. While the source of the reduced bond strength is not readily deduced, the dramatic effect on the S−H BDE suggests that design of highly reactive thiols can be envisioned for heterogeneous and homogeneous hydrogen transfer. Finally, from the data of Table 4, the thermochemical cycle for reaction of hydrogen with the **Fe_2S_2** system is estimated (Scheme 6). Loss of a single hydrogen atom from **$Fe_2S_2H_2$** occurs with $\Delta H^\circ = 73$ kcal/mol to form **$Fe_2S_2H^{\bullet}$**. Loss of the second hydrogen atom is predicted to occur

(48) Lu, X. Q.; Zhu, C. Y.; Song, L. C.; Chen, Y. T. *Inorg. Chim. Acta* **1988**, *143*, 55–57.

(49) Peters, W. J.; Lanzillota, W. N.; Lemon, B. J.; Seefeld, L. C. *Science* **1998**, *282*, 1853.

Chart 3. Relative Stabilities, (Enthalpies, 298 K), [Free Energies, 298 K] of Isomers of **$Fe_2S_2H_2$** and **Fe_2S_2MeH** and Radicals **$Fe_2S_2H^\bullet$** and **$Fe_2S_2Me^\bullet$**, All in kcal/mol

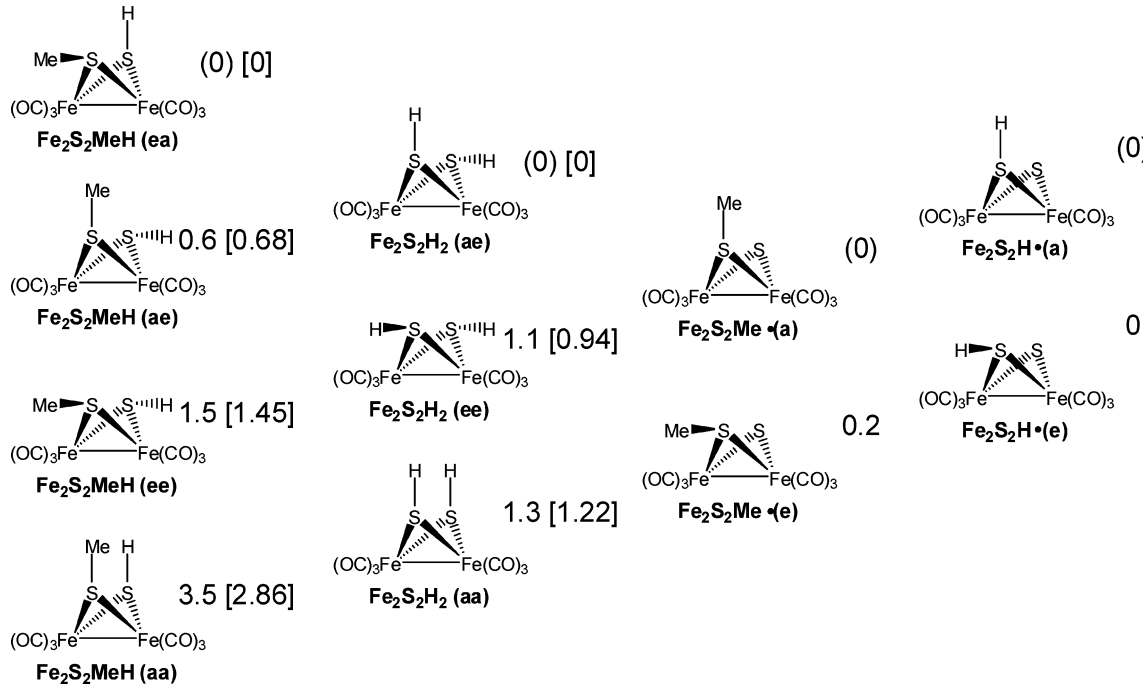

Table 5. Computed Bond Dissociation Energies [$\Delta H°$(298 K), kcal/mol] for Geometries Optimized at ROB3LYP/CEP-121G ECP on Fe and 6-311++G(2d,2p) on C, H, S, and O

reaction	XS−H → XS• + H•
$Fe_2S_2H_2$ (ae) → **$Fe_2S_2H^\bullet$ (a)** + H•	73.1
Fe_2S_2MeH (ea) → **$Fe_2S_2Me^\bullet$ (e)** + H•	73.2
Fe_2S_3MeH (ae) → **$Fe_2S_3Me^\bullet$ (a)** + H•	72.8
$Fe_2S_2(CO)MeH$ (ae) → **$Fe_2S_2(CO)Me^\bullet$ (a)** + H•	66.2

Table 6. DFT Geometries of **Fe_2S_3MeH** (**ea**) and **$Fe_2S_3Me^\bullet$** (**e**)

	Fe_2S_3MeH (ea)	**$Fe_2S_3Me^\bullet$**
Bond Distances, Å		
Fe(7)−Fe(1)	3.06	3.157
Fe(7)−S(16)	2.356	2.339
Fe(7)−S(14)	2.39	2.381
Fe(7)−S(15)	2.389	2.334
S(14)−C(18)	1.832	1.835
S(15)−H(22)	1.348	
S(14)−S(16)	3.221	3.213
S(14)−S(15)	3.099	3.111
Angles, deg		
Fe(7)−S(16)−Fe(1)	81	84.9
Fe(7)−S(15)−Fe(1)	79.7	85.1
Fe(7)−S(14)−Fe(11)	79.7	83.1

with $\Delta H° = 47$ kcal/mol. Overall dihydrogen addition to **Fe_2S_2** occurs with $\Delta H° = -16$ kcal/mol.

Correlation of Benzyl Radical Abstraction Rates and BDEs. With BDEs in hand, the relationship between $\ln(k_{abs})$ and the S−H BDE for the thiols and hydrosulfides in Table 1 may be explored in the form of a Polanyi correlation, as shown in Figure 8. The Polanyi correlations are useful for predicting rates from enthalpy changes for closely related series of hydrogen-transfer reactions, in the absence of significant changes in polar and steric effects across a series of donors. Donors with BDEs varying from 91.2 kcal/mol (H_2S) to 74.2 kcal/mol (the **Fe_2S_2MeH** thiol) appear reasonably well correlated. However, a notable outlier is Cp*Mo(μ-S)$_2$(μ-SH)(μ-SCH$_3$)MoCp* (BDE = 71 kcal/mol), for which the hydrogen atom abstraction rate is a factor of 10 slower than that for **Fe_2S_2MeH** (BDE =74 kcal/mol). This must reflect steric retardation of the abstraction reaction by [Cp*Mo(μ-SH)(μ-SCH$_3$)(μ-S)$_2$]$_2$, as the benzyl radical is constrained to enter a channel between the Cp* rings to abstract the S−H atom. This Polanyi relation predicts that **$Fe_2S_2(CO)MeH$** (S−H BDE = 66 kcal/mol) will donate a hydrogen atom to the benzyl radical with a bimolecular rate constant of 4.5×10^8 M^{-1} s^{-1} at 298 K, a factor of 4 slower than diffusion control. Thus, activation of the hydrosulfido group in the Fe(μ-SH)Fe structure, reminiscent of the Mo(μ-SH)Mo cluster, can be designed and modified to produce bond strengths near the range of organometallic M−H bond strengths, with reaction rates with carbon-centered radicals approaching diffusion control, and capable of donating S−H hydrogen atoms to π-acceptors at appreciable rates near ambient temperature.

Table 7. DFT Geometries for **$Fe_2S_2(CO)MeH$** and **$Fe_2S_2(CO)Me•$**

	$Fe_2S_2(CO)MeH$	**$Fe_2S_2(CO)Me^\bullet$**
Bond Distances, Å		
Fe(7)−Fe(1)	2.991	2.78
Fe(7)−C(15)	2.028	2.051
Fe(7)−S(16)	2.419	2.35
Fe(7)−S(14)	2.392	2.395
S(14)−C(18)	1.835	1.831
Angles, deg		
Fe(7)−C(15)−Fe(1)	95.01	85.3
Fe(7)−S(16)−Fe(1)	76.36	72.5
Fe(7)−S(14)−Fe(1)	77.39	70.9
O(22)−C(15)−Fe(7)	137.3	132.5

Summary and Conclusions

The S−H bond strength for (OC)$_3$Fe(μ-SCH$_3$)(μ-SH)Fe(CO)$_3$ has been determined; it is the first measured for Fe(μ-SH)Fe structures. The first absolute rate expressions have been determined for reaction of a carbon-centered benzyl radical with the activated hydrosulfido group in these iron sulfide complexes.

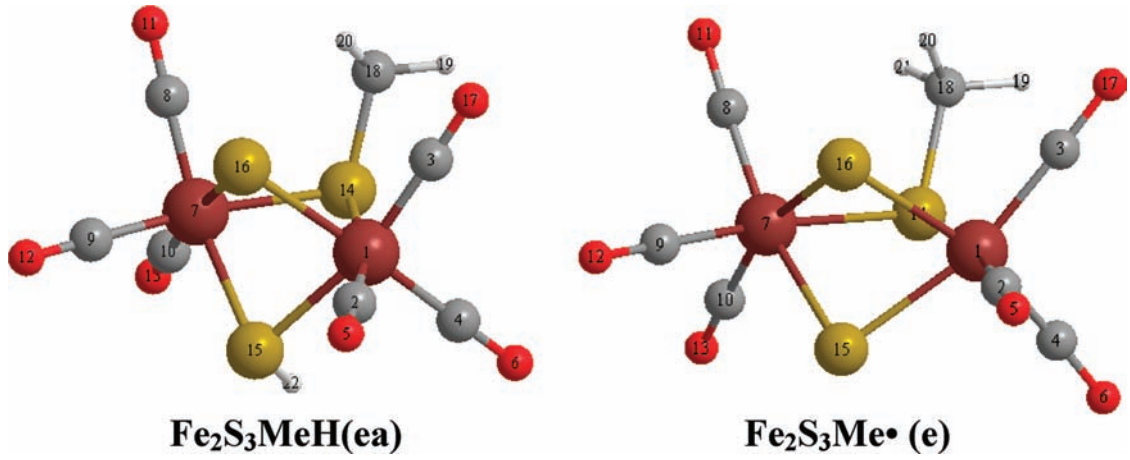

Figure 6. DFT structures of (left) the parent hydrosulfide **Fe_2S_3MeH** (**ea**) and (right) the resulting radical **Fe_2S_3Me•** (**e**).

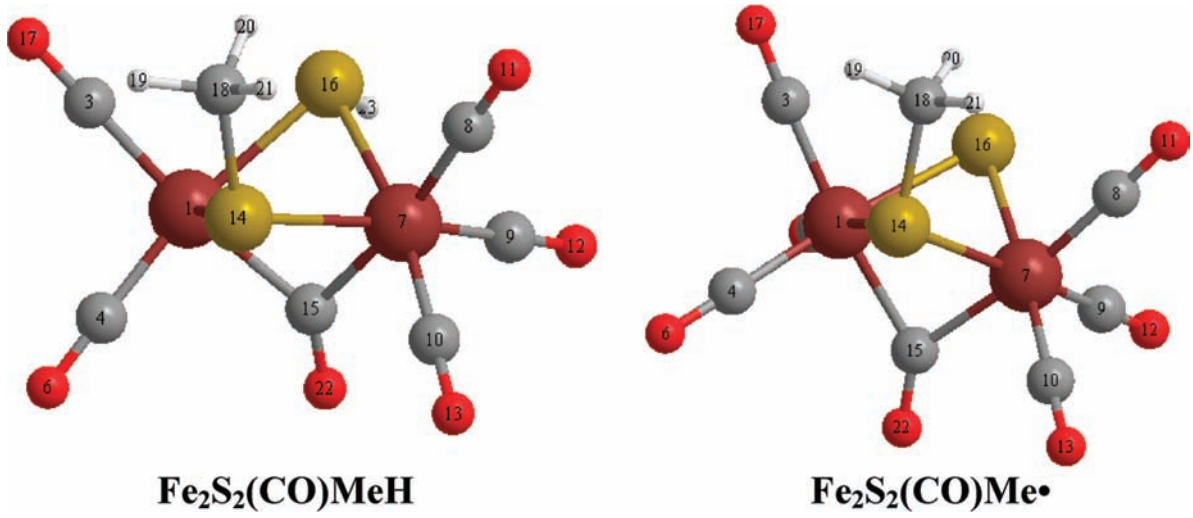

Figure 7. DFT structures of (left) the parent hydrosulfide **Fe_2S_2(CO)MeH** and (right) the resulting radical **Fe_2S_2(CO)Me•**.

Scheme 6. Thermochemical Cycle for the Addition of Dihydrogen and Subsequent Hydrogen Atom Losses for **Fe_2S_2**[a]

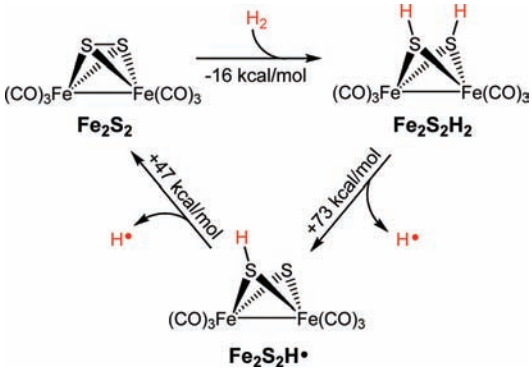

[a] Note that the sum of the energies of the steps is equal to the homolytic bond strength for dihydrogen.

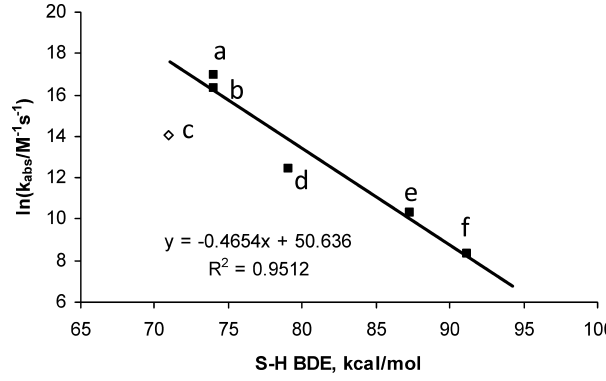

Figure 8. Polanyi[50] plot of $\ln(k_{abs}/M^{-1}\ s^{-1})$ versus S−H bond strength (kcal/mol) for reaction of benzyl radical with thiol donors in benzene, 298 K, $\ln(k_{abs}/M^{-1}\ s^{-1}) = (-0.465 \pm 0.07)(BDE) + 50.6 \pm 5.0$ (1σ error, $R^2 = 0.95$), $\Delta H°$ is the S−H bond strength of the thiol. The data are equivalently plotted as $\ln(k_{abs}/M^{-1}\ s{-}1) = (-0.465)(\Delta BDE) + 9.2$, where ΔBDE is the difference in BDE between toluene, 89 kcal/mol, and the thiol. (a) **$Fe_2S_2H_2$**, (b) **Fe_2S_2MeH**, (c) Cp*Mo(μ-SCH_3)(μ-SH)(μ-S)$_2$Cp* (◇, not included in correlation), (d) **PhSH**, (e) octanethiol, and (f) **H_2S**.

Activation of the hydrosulfido groups leads to enhancement in hydrogen-donating rates of 10^2-10^3-fold over those of alkanethiols and H_2S, and with suitable substitution, a predicted (Polanyi) enhancement of hydrogen abstraction rates up to 10^5-fold over that of H_2S is achievable. As in the case of Mo(μ-SH)Mo systems, S−H bond strengths in Fe(μ-SH)Fe systems span a range overlapping metal−hydride bond strengths. For the present iron systems, the (RO)B3LYP method employed here appears to give quite satisfactory results in predicting S−H bond strengths, thermodynamic populations, and NMR properties of the Fe(μ-SH)Fe structures. Finally, the present results illustrate that Fe(μ-SH)Fe bond strengths can be designed to

be sufficiently low to make possible the participation of the S−H bond in selective hydrogenation of acceptor π systems, consistent with the retro-disproportionation mode of hydrogen transfer from Fe(μ-SH)Fe to aromatic π acceptors, and the bond strengths of designed Fe(μ-SH)Fe systems may be low enough to enable re-initiation in controlled polymerization.

Experimental Procedures

Instrumentation. Electrochemical data were collected in 0.3 M NEt_4BF_4 in acetonitrile using a CH Instruments model 660C computer-aided three-electrode potentiostat. The working electrode was either a glassy carbon or platinum disk, the counter electrode was a glassy carbon rod, and a silver chloride coated silver wire was used as a pseudo-reference electrode and was separated from the main compartment by a Vycor disk (1/8 in. diameter) obtained from Bioanalytical Systems, Inc. Ferrocene or decamethylferrocene was used as an internal reference, with all potentials reported versus the ferricenium/ferrocene couple.

Materials. Reagents were purchased commercially and used without further purification unless otherwise specified. All reactions, syntheses, and manipulations of Fe_2S_2 complexes were carried out under nitrogen using standard Schlenk techniques or in a glovebox. Acetonitrile was dried by activated alumina column in an Innovative Technology, Inc. PureSolv system. CD_3CN was dried over activated sieves, degassed, and stored in a glovebox. Benzene for photolysis experiments was triply fractionally distilled to reduce trace toluene to $\sim 10^{-7}$ M. Dibenzyl ketone (DBK) was recrystallized from methanol.

Preparation of $Fe_2S_2H_2$. Following the procedure of Seyferth et al.,[51] $\mathbf{Fe_2S_2H_2}$ was prepared from $\mathbf{Fe_2S_2}$. The crude product was dissolved in warm hexane, insoluble particulates were removed by filtration, and the soluble fraction was recrystallized under an inert atmosphere. The ^{1}H NMR spectrum revealed a mixture of axial−equatorial, axial−axial, and equatorial isomers similar to the ratio reported. $\mathbf{Fe_2S_2H_2}$ was found to have a shelf life of a few days at room temperature; it was stored in a freezer and recrystallized from hexane as necessary, and its thiol content was assayed by ^{1}H NMR immediately prior to use.

Preparation of Fe_2S_2MeH. Following the method of Seyferth and co-workers,[52] methyllithium (1.8 mL of 1.6 M in Et_2O, 2.9 mmol) was added via syringe into a red solution of 2.91 mmol of $\mathbf{Fe_2S_2}$ in THF at −78 °C. The red solution became green upon formation of the anion, $\mathbf{Fe_2S_2Me^-}$. The green mixture was stirred for 1 h. Addition of trifluoroacetic acid (0.22 mL, 2.9 mmol) to the mixture at −78 °C restored a deep red color. The mixture was continuously stirred for an additional 1 h and slowly warmed to room temperature. The solvent was removed, and the red solid was dried under vacuum. The product was recrystallized from pentane to give a highly pure mixture of two isomers in 75% yield in a 5:1 ratio. ^{1}H NMR (C_6D_6, 500 MHz): δ 1.40 and 1.39 (s, 3.0 H total, SCH_3, isomers A and B), δ −1.16 (s, 0.12 H, SH, isomer B), −2.86 (s, 0.73 H, SH, isomer A).

Preparation of Fe_2S_2MeBz. Methyllithium (0.2 mL of 1.6 M in Et_2O, 3.2 mmol) was added via syringe into a solution of $\mathbf{Fe_2S_2}$ (0.100 g, 0.29 mmol) in THF (20 mL) at −78 °C following the procedure of Seyferth.[53] The reaction mixture changed from orange to dark green, indicating the formation of $\mathbf{Fe_2S_2Me^-}$. After the reaction was stirred for 30 min, 35 μL of benzyl bromide was added, and the mixture was slowly warmed to room temperature. The solution changed from green to reddish-brown at about 10 °C. The mixture was stirred at room temperature for an additional 30 min, and the solvent was removed under vacuum, leaving a red-orange oil. The crude product was extracted with pentane to yield 53 mg of product (41% yield). ^{1}H NMR (C_6D_6, 500 MHz): δ 1.41 (s, 0.9 H, CH_3, isomer 1), 1.55 (s, 2.1 H, CH_3, isomer 2), 2.73 (s, 0.63 H, CH_2, isomer 1), 2.99 (s, 1.37 H, CH_2, isomer 2), 7.00 (m, 5 H, C_6H_5, both isomers).

Kinetics of Reaction of Benzyl Radical and $Fe_2S_2H_2$. Stock solutions of 1×10^{-4} M $\mathbf{Fe_2S_2H_2}$ and *tert*-butylbenzene (GC standard) and 0.02 M dibenzyl ketone were dissolved in degassed benzene, and 100-μL samples were freeze−thaw degassed and sealed in Pyrex tubes. The samples were thermostatted in a temperature-controlled hexadecane bath equipped with a quartz optical window. Photolysis was carried out with the diffuse light of a 1000-W Hanovia high-pressure xenon lamp filtered through a water filter, over periods of 0.5 s, with less than 5% conversion of $\mathbf{Fe_2S_2H_2}$, by means of a computer-controlled electronic shutter, Uniblitz model 225L0A0T522952. Kinetics were measured from 299 to 345 K. Samples were opened, and toluene and bibenzyl concentrations were determined by capillary gas chromatography. Concentrations of products and $\mathbf{Fe_2S_2H_2}$ were corrected for temperature using the relation $\rho_T = 1.192 - 1.059 \times 10^{-3}$ K g/mL for the temperature dependence of the density of benzene.[54]

Self-Diffusion Coefficients of Fe_2S_2 in Benzene. Self-diffusion coefficients for $\mathbf{Fe_2S_2}$ in benzene were measured as a model for the self-reaction rates of radical $\mathbf{Fe_2S_2H^\bullet}$ by the Taylor method,[55] over the range 20−53 °C. The apparatus consisted of a Waters HPLC pump delivering flow through a 20-cm normal-phase silica column to dampen pressure oscillations, followed by a Waters HPLC injector attached to a 31.7-m long, internal radius 0.052 cm, PEEK column thermostatted in a Neslab RTE-211 water bath. Analysis of the effluent was carried out with a Waters model 2410 refractometer. The variance (σ^2) of the eluted peak for $\mathbf{Fe_2S_2}$ was determined by measuring the full-width at half height, $\Gamma = 2.345\sigma$. The relationship between the internal radius of the coiled tube, r, the retention volume t, σ^2, and the diffusion coefficient, D, is given by $D = r^2t/24\sigma^2$. Laminar flow was confirmed by reducing the column flow rate until measured values of D were constant, achieved at a flow rate of 0.3 mL/min. The resulting diffusion coefficients for $\mathbf{Fe_2S_2}$ in benzene were (10^{-5} cm^2/s): 20 °C, 1.338, 1.282; 28 °C, 1.535, 1.526; 40 °C, 1.87, 1.95; 53 °C, 2.327, 2.301.

Estimation of Self-Termination Rates for $Fe_2S_2H^\bullet$ and Cross-Termination Rates for the Reaction of Benzyl Radical with $Fe_2S_2H^\bullet$. The above-measured values of self-diffusion of $\mathbf{Fe_2S_2}$ were employed as a model for diffusion of $\mathbf{Fe_2S_2H^\bullet}$, using the classical von Smoluchowski equation for self-termination, $2k_t = (8\pi/1000)\sigma\rho N D_{AB}$, where $\sigma = 1/4$, the fraction of encounter pairs undergoing reaction, assuming slow intersystem crossing of singlet and triplet cage radical pairs of $\mathbf{Fe_2S_2H^\bullet}$, ρ is the reaction diameter, $(7.53 \pm 0.25) \times 10^{-8}$ cm, estimated for $\mathbf{Fe_2S_2H^\bullet}$ using Spernol−Wirtz,[56] van der Waals,[57] and LeBas[58] methods (or from the molecular volume of $\mathbf{Fe_2S_2}$ estimated by PCModel[59]), $N = 6.022 \times 10^{23}$ (Avogadro's number), and D_{AB} are experimental diffusion coefficients of $\mathbf{Fe_2S_2}$, the model for $\mathbf{Fe_2S_2H^\bullet}$. This results in an expression for the total self-termination rate for $\mathbf{Fe_2S_2H^\bullet}$:

(50) (a) Gardner, K. A.; Kuehnert, L. A.; Mayer, J. M. *Inorg. Chem.* **1997**, *36*, 2069–2078. (b) Ingold, K. U. In *Free Radicals*; Kochi, J. K., Ed.; Wiley: New York, 1973; Vol. *1*, Chapter 2, p 69. (c) Russell, G. A. In *Free Radicals*; Kochi, J. K., Ed.; Wiley: New York, 1973; Vol. *1*, Chapter 7, pp 283−293. (d) Tedder, J. M. *Angew. Chem., Int. Ed. Engl.* **1982**, *21*, 401–410. (e) Korzekwa, K. R.; Jones, J. P.; Gillette, J. R. *J. Am. Chem. Soc.* **1990**, *112*, 7042–7046.

(51) Seyferth, D.; Womack, G. B.; Hendersen, R. S. *Organometallics* **1986**, *5*, 1568–1575.

(52) Seyferth, D.; Henderson, R. S.; Song, L.; Womack, G. B. *J. Organomet. Chem.* **1985**, *292*, 9–17.

(53) (a) Seyferth, D.; Henderson, R. S. *J. Am. Chem. Soc.* **1979**, *101*, 508–509. (b) Seyferth, D.; Henderson, R. S.; Song, L.-C.; Womack, G. B. *J. Organomet. Chem.* **1985**, *292*, 9–17. (c) Song, L.-C. *Acc. Chem. Res.* **2005**, *38*, 21–28.

(54) Reid, R. C.; Prausnitz, J. M. Sherwood, T. K. *The Properties of Gas and Liquids and Gases*; McGraw-Hill: New York, 1977.

(55) Taylor, G. *Proc. R. Soc. London, Ser. A* **1954**, *235*, 473.

(56) Spernol, A.; Wirtz, K. *Z. Naturforsch.* **1953**, *8a*, 522.

(57) Edward, J. T. *J. Chem. Educ.* **1970**, *47*, 261.

(58) Ghai, R. L.; Dullien, F. A. L. *J. Phys. Chem.* **1974**, *78*, 2283.

(59) *PCMODEL*, version 9.1; Serena Software: Bloomington, IN, 2002.

$$\ln(2k_t'/M^{-1}\,s^{-1}) = 27.8 - 3359.6/RT \quad (R = 1.9872 \text{ and } T, \text{K})$$

To estimate the *cross-termination* rate constants for reaction of benzyl radical and **$Fe_2S_2H^{\bullet}$**, rate constants for self-termination of benzyl radical in benzene, given by $\ln(2k_t/M^{-1}\,s^{-1}) = 27.23 - 2952.5/RT$, were combined with the above expression for self-termination of **$Fe_2S_2H^{\bullet}$**, utilizing the relationship $2k_{ct} = 2(k_tk_t')^{1/2}$. The basis for using twice the geometric mean of self-termination rate constants for estimation of cross-termination constants has been addressed in detail.[60] The resulting rate expression is given by

$$\ln(2k_{ct}/M^{-1}\,s^{-1}) = 28.21 - 3156.1/RT$$

Calculation of Rate Constants for Reaction of $Fe_2S_2H_2$ and Benzyl Radical. In the case of **$Fe_2S_2H_2$**, kinetic modeling suggests that a significant portion (ca. one-third) of the total toluene was formed from **$Fe_2S_2H^{\bullet}$** by disproportionative cross-termination (eq 5). Photolysis of DBK in the presence of **$Fe_2S_2H_2$** revealed (by NMR) no formation of combination cross-termination products **Fe_2S_2BzH** or the self-termination combination product **$(Fe_2S_2H)_2$**. The lack of **Fe_2S_2BzH** or **$(Fe_2S_2H)_2$** suggests that disproportionation pathways dominate self-termination reactions. The portion of toluene formed in disproportionation, eq 5, can be calculated by numerical integration of eqs 2a−5 and 7 with neglect of eqs 6 and 8 using termination rate constants available from the von Smoluchowski treatment of the self-diffusion of **$Fe_2S_2H^{\bullet}$**, as illustrated above. Thus, the rate constants k_{abs} (eq 2) were determined by numerical integration of eqs 2−5 and 7 with k_{abs} as the sole variable. Inputs for the numerical integration and optimization were as follows: For eqs 2a and 2b, the rate of photolysis of DBK is given by ([toluene]/2 + [bibenzyl])/Δt, where Δt is the duration of photolysis, 0.5 s. The value of k_{abs} was the optimized variable in the numerical integration. For eq 4, k_t was calculated from the expression $\ln(2k_t/M^{-1}\,s^{-1}) = 27.23 - 2952.5/RT$. For eq 5, based on the lack of cross-combination product **Fe_2S_2BzH**, all cross-termination is assigned to eq 5, with k_{ct} given by $\ln(2k_{ct}/M^{-1}\,s^{-1}) = 28.21 - 3156.1/RT$, and eq 6 is neglected. From the absence of product **$(Fe_2S_2H)_2$**, the self-termination of **$Fe_2S_2H^{\bullet}$** is assigned entirely to eq 7, and eq 8 is neglected. The disproportionative self-termination rate of **$Fe_2S_2H^{\bullet}$** is estimated from the experimental self-diffusion coefficients of **Fe_2S_2**, as described above, and is given by $\ln(2k_t'/M^{-1}\,s^{-1}) = 27.8 - 3359.6/RT$. For each experiment, experimental inputs for numerical integration include the observed concentrations of toluene and bibenzyl, the initial concentration of **$Fe_2S_2H_2$**, the rate of photolysis of DBK (= ([toluene]/2 + [bibenzyl])/Δt, typically $(1.3 \pm 0.5) \times 10^{-5}$ M s^{-1}, and the duration of photolysis, $\Delta t = 0.5$ s. Equations 2−6 are numerically integrated with optimization of k_{abs} using the Berkeley Madonna[61] program while holding constant the values of k_t, k_t', and k_{ct} from the expressions developed above. A fourth-order Runge−Kutta integration routine was used with time increments of 1×10^{-7} s. Values of k_{abs} are varied in the optimization to fit experimental bibenzyl and toluene concentrations. Under the present conditions, it was found that values of k_{abs} are reduced by ca. 35% by taking cross-termination into account compared to the neglect of cross-termination of benzyl radical with **$Fe_2S_2H^{\bullet}$** (eq 5). A sensitivity test of the error in k_{abs} as a function of error in k_t, k_{ct}, and k_t' was carried out; an error of 100% in either of the latter two termination rate constants results in less than 10% error in k_{abs}.

(60) (a) Münger, K.; Fischer, H. *Int. J. Chem. Kinet* **1984**, *16*, 1213. (b) Paul, H.; Segaud, C. *Int. J. Chem. Kinet.* **1980**, *7*, 637. (c) Fischer, H.; Paul, H. *Acc. Chem. Res.* **1987**, *20*, 200.

(61) Macey, R. I.; Oster, G. F. *Berkeley Madonna*, version 8.0.1; 2000; http://www.berkeleymadonna.com/.

Kinetics of Reaction of Benzyl Radical with Fe_2S_2MeH and Calculation of Rate Constants. One-hundred-microliter samples of a solution of **Fe_2S_2MeH** (3.2×10^{-5} M), dibenzyl ketone (0.02 M), and *tert*-butylbenzene (5.2×10^{-4} M, GC standard) in benzene were freeze−thaw degassed, sealed in 5-mm-o.d. × 5-cm Pyrex tubes, and photolyzed for 1 s with diffuse light from a 1-kW high-pressure Xe lamp and computer-controlled optical shutter as described above. Under these conditions, the photolysis of dibenzyl ketone occurs at ca. 1.5×10^{-5} M/L·s. Rate constants were calculated according to eq 8 from the concentrations of toluene and bibenzyl, photolysis time, and k_t values determined from the expression $\ln(2k_t/M^{-1}\,s^{-1}) = 27.23 - 2952.5/RT$. Results are given in Table 1.

Photolysis of Fe_2S_2MeH with DBK in C_6D_6 for Product Analysis. A stock solution was prepared to be 2.7 mM of **Fe_2S_2MeH** and 0.2 M of DBK in C_6D_6. The stock solution was diluted by a factor of 10 and divided into 10 NMR tubes for photolysis. Each tube was photolized for 2 s, and then all 10 samples were combined and condensed by evaporation to 1 mL for analysis by ^{1}H NMR. The two methylene resonances for the benzylthiolate groups observed in the ^{1}H NMR spectrum match the resonances of the authentic **Fe_2S_2MeBz** at 2.73 and 2.99 ppm. The methanethiolate resonances, however, could not be cleanly observed due to overlap with the signals for the starting material, **Fe_2S_2MeH**.

Kinetics of Reaction of Benzyl Radical and H_2S. On a vacuum line, ca. 15 mL samples of gaseous H_2S (1 atm) were condensed into 200-μL samples of a benzene-d_6 solution of dibenzyl ketone (0.02 M), *tert*-butylbenzene (0.001 M), and hexamethylbenzene (0.02 M) in 3-mm Pyrex tubes, freeze−thaw degassed, and sealed. After sealing, the samples, having 300 μL of head space above the liquid phase, were placed in standard 5-mm NMR tubes and equilibrated at the desired photolysis temperature to constant H_2S concentrations, as determined by careful integration of the H_2S peak relative to *tert*-butylbenzene and hexamethylbenzene internal standards. H_2S exhibits long T_1 (ca. 30 s) values, necessitating long recycle times: 45° ^{1}H pulse widths and 120-s delays were employed. The samples required up to 4 h for H_2S concentrations to fully equilibrate. The samples were placed into a thermostatted hexadecane photolysis bath and photolyzed for 1−15 s. Rate constants were calculated according to eq 1.

Determination of pK_a by NMR. In a typical experiment, **Fe_2S_2MeH** and 2,4,6-trimethylpyridine (10.8 and 9.2 mmol, respectively) were mixed in 1.0 mL of CD_3CN. Due to rapid proton exchange, the chemical shifts observed for each species were the weighted averages of the chemical shifts for the protonated and deprotonated species. Using the known pK_a of 2,4,6-trimethylpyridine (14.98),[31] the ratio of 2,4,6-trimethylpyridine to 2,4,6-trimethylpyridinium from the chemical shift (3.29:1), and the 1:3.55 ratio of **$Fe_2S_2Me^-$** to **Fe_2S_2MeH** (the anion to the neutral S−H) gives a pK_a of 16.0 ± 0.4 from four independent equilibrium determinations (the listed error is $2\sigma + 0.2$ to account for the reproducibility and any error in the reference base). Details of the pK_a determination are shown in the Supporting Information.

Cyclic Voltammetry. Solutions of **Fe_2S_2MeH** were prepared at 0.5 and 1.5 mM in 0.3 M NEt_4BF_4 in acetonitrile. The anion, **$Fe_2S_2Me^-$**, was generated *in situ* by adding 1 equiv of triethylamine. The anodic peak potential (E_{pa}) for the resulting irreversible oxidation was observed between −0.39 and −0.29 V vs $FeCp_2$ over the range 0.05−100 V/s. Simulations of the CVs were run using DigiSim[33] with a one-electron oxidation, followed by dimerization with a diffusion-controlled rate constant of 2×10^9 $M^{-1}\,s^{-1}$, based upon the previously reported dimer synthesis for the phenyl analogue.[32] For each concentration and scan rate, the difference between the $E_{1/2}$ and the resulting irreversible E_{pa} was used to correct the experimental data to give an average $E_{1/2}$ of −0.26 ± 0.05 V vs ferrocene (where the listed error is 2σ + 10 mV to account for the reproducibility of the

measurement and correction of the potential, as well as any error in the reference).

Acknowledgment. Work at Pacific Northwest National Laboratory (PNNL) was supported by the Division of Chemical Sciences, Office of Basic Energy Sciences, U.S. Department of Energy (DOE). Battelle operates PNNL for DOE. Provision of computational resources at the National Energy Research Scientific Computing Facility (NERSC) by the Office of Science, U.S. DOE, is gratefully acknowledged. This paper is dedicated to Keith U. Ingold on the occasion of his 80th birthday.

Supporting Information Available: Tables of the kinetic data, detailed summaries of DFT calculations, details of the pK_a determination, and complete ref 39. This material is available free of charge via the Internet at http://pubs.acs.org.

JA904602P